Diachronic UAV study of coastal badlands supported by geophysical imaging in the context of accelerated erosion processes

Cyrille Fauchard, Vincent Guilbert, Raphael Antoine, Cyril Ledun, Bruno Beaucamp, Olivier Maquaire, Stéphane Costa, Mohand Medjkane, Thomas Roulland

Technical Note

Landslides
DOI 10.1007/s10346-022-02006-2
Received: 24 January 2022
Accepted: 28 November 2022

Cyrille Fauchard · Vincent Guilbert · Raphael Antoine · Cyril Ledun · Bruno Beaucamp · Olivier Maquaire · Stéphane Costa · Mohand Medjkane · Thomas Roulland

Diachronic UAV study of coastal badlands supported by geophysical imaging in the context of accelerated erosion processes

Abstract This work presents a 4-year study carried out on the so-called Vaches Noires cliffs (VNCs), in Normandy, France, between April 2016 and January 2019. The VNCs are badlands facing the Channel sea, with Cretaceous to Jurassic formations. They are subject to strong erosion processes already described by former works. This study aims to gain greater insight into the erosion phenomena with the help of aerial surveys supported by geophysical imaging. For this purpose, Digital Elevation Models (DEMs) were established using photogrammetry applied to dozens of photos taken by an Unmanned Aerial Vehicle (UAV). Electrical Resistivity Imaging (ERI) was implemented according to profiles that were both transverse and parallel to the coastline, (i) from the top to bottom of the cliffs, (ii) as well as at the toe of the crests and on the beach. The main outcome is a global methodology to properly perform these methods and to combine all the results in a 3D environment using free software. This methodology was validated according to a 1-year experiment based on the comparison of two DEMs, then extended to a 4-year diachronic approach. Moreover, volumes of eroded and deposited materials were assessed in specific, morphodynamic areas of the cliffs. The ERI results were used to carry out thickness assessments of the layers involved in the erosion process, and served to clarify the local geology; however, their interpretation remains limited by the lack of a priori information, and underlines the need to carry out inversion processes via a 3D approach in a particularly complex topography. In conclusion, this work provides effective tools to anticipate the risks that threaten coastal habitats and infrastructures, and represents a solid basis for further study.

Keywords Drone · Electrical resistivity imaging

Introduction

Landslides are natural processes, resulting from ecosystem evolution and development (Gonzalez-Ollauri and Mickovski 2017). As human habitats and economic activities extend across territories, landslides have become hazards that may threaten human life and infrastructures. In the context of global climate change, hazards are on the increase while major meteorological events are tending to accelerate. Moreover, landslides on coastal cliffs can be amplified by rising sea levels. Consequently, mitigating the associated risks is a priority for stakeholders involved in territorial planning. Predicting gravitational movements or assessing a mass that may potentially slide falls within the sphere of classic Earth sciences problems. Moreover, it is widely acknowledged that a combination of scientific disciplines, using aerial and terrestrial data, represents the ideal response (Viles 2016).

In this work, we focus on a part of the badlands coastal system referred to as the "Vaches Noires" cliffs (VNCs) in Normandy, France. The VNCs are subject to rapid erosion already described by (Maquaire et al. 2013; Quinejure 1971; Medjkane et al. 2018), resulting from a combination of landslides, hydrogeological or tidal phenomena (solifluction and washout) leading to a significant retreat at the top, a variable coastline at the toe, a global erosion of crests and secondary scarp, and an unknown balance of sedimentary deposition several kilometers offshore (Roulland et al. 2019, 2021). The consequences are twofold: (i) public territories are exposed to dramatic events that threaten inhabitants and infrastructures, and (ii) sedimentary deposits generate important dredging costs borne by the harbor of Le Havre and the Seine waterway's stakeholders. Tackling these two key issues is therefore of paramount importance. Moreover, against a backdrop of climate change, the VNCs represent an ideal landslide case study in the field of coastal research where hydrogeological erosion processes are amplified by the rising ocean levels and an acceleration of meteorological events such as severe storms.

The Digital Elevation Model (DEM) is one of the key methods for studying surface changes in a landscape (Hirt et al. 2010). The DEM is computed from a point cloud of the observed surface using various Geographical Information System (GIS) software solutions. DEM data are structured according to a grid (regular, triangular or contours (Prodanovic 2002)and can be easily implemented on a computer. The main outcomes are usually distance and volume comparisons between at least two DEMs (Fuller et al. 2009), at various time intervals, depending on the speed at which the phenomena observed develop. In the steepest reliefs or on rough surfaces, the DEM comparison may prove inaccurate. An alternative approach consists in performing comparisons directly between point clouds, without the need for meshing the surface data (Barnhart and Crosby 2013; Lague et al. 2013).

The Terrestrial Laser Scanner (TLS) based on the LiDAR (Light/Laser Detection And Ranging) technology and the Structure from Motion (SfM) based on photogrammetry are the two main methods used to obtain a point cloud. Both can be carried out on the ground or from the air, and provide the surface topography for various applications in the geomorphological domain (Hobbs et al. 2020; Letortu et al. 2019; Milan et al. 2007; Rosser et al. 2005).

Nevertheless, while TLS offers a satisfactory level of accuracy for positioning, the TLS location on the ground can limit the method when faced with a complex topography (Gruszczynski et al. 2017)due to the occlusion of some parts of the relief. Terrestrial SfM appears less cost-effective (Goncalves and Henriques 2015)and can be less accurate in positioning than TLS. Finally, even if multiple terrestrial SfM points of view can be selected, complex topography remains a problem since some parts of the surveyed surface can be hidden and not accessible, as in the TLS method. Work conducted by (Medjkane et al. 2018) proposed a diachronic study of the VNCs site using a TLS system and SfM. Both methods were implemented on the beach, facing the cliffs to be monitored. Dozens of TLS and SfM DEMs were compared and the results were mostly satisfactory; however, some parts of the cliffs were not correctly measured due to occlusions and they were inaccessible by foot. A smart alternative consists in surveying the terrain from the air by means of a UAV or drone.

Extensive work on the use of UAVs in engineering geology and Earth sciences has been recently proposed by (Giordan et al. 2020; Antoine et al. 2020). UAVs offer the possibility of surveying a given surface according to a flight plane, at a given height, with LiDAR technology. Nevertheless, the use of a visible camera for photogrammetric surface reconstruction is on the increase since it represents a lower-cost solution that yields results as accurate as those provided by LiDAR (Casella et al. 2014; Chesley et al. 2017; Rossi et al. 2018) and shows how photogrammetry using UAVs is an efficient and low-cost solution for assessing mass movements at intermediate observation scales between on-site and other types of aerial surveys (plane, satellite).

An important issue in DEM obtained by photogrammetry is that it relies on the georeferencing of point clouds. (Turner et al. 2016) remarked that recent advances in UAV technology offer the ability to have an on-board Real Time Kinematic - Global Navigation Satellite System (RTK-GNSS), providing an accurate localization of recorded images. Nevertheless, this system remains rare and georeferenced localization on the ground is generally performed by terrestrial Differential GNSS (DGNSS) at specific points called Ground Control Points (GCP) (Agüera-Vega et al. 2017).

Once the DEM has been built and georeferenced, the common approach may consist in surveying the subsurface with the help of geophysical and geotechnical methods, since the events that trigger landslides are strongly dependent on the soil nature, its mechanical properties and its hydrology. Electrical Resistivity Imaging (ERI) is one of the most widely used techniques to investigate landslide subsurface. A very detailed review on this topic was presented in 2014 by (Perrone et al. 2014)and more recently, by (Pazzi et al. 2019; Whiteley et al. 2019). Most reported landslide studies (2D, 3D and monitoring) concern a sedimentary context involving clay, marl or limestone formations and, to a lesser extent, fractured magmatic and metamorphic rocks. Indeed, ERI has a wide range of applications since the method is sensitive to conductive (clay) as well as resistive (rock) materials (Telford et al. 1990).

Other geophysical methods combined with ERI offer an enhanced interpretation (Göktürkler et al. 2008; Grandjean et al. 2011; Petronio et al. 2016). Very close to the VNCs, (Fressard et al. 2016)studied the Bas Verger landslide using ERI, geotechnical testing and aerial photos taken at different times to establish the morphodynamic map and describe the various phenomena that trigger landslides. (Chambers et al. 2011)presented a combined approach with ERI, Self Potential (SP), Automated Resistivity Profiles (ARP) and auger logs to draw geomorphodynamic maps and associate surface and internal phenomena. Another nearby site (Cirque des Graves) was studied by (Lissak et al. 2014)by means of ground-based and aerial data. A geomorphological analysis was proposed taking into account LiDAR, geotechnical, electrical and seismic measurements. (Boon et al. 2015) used geomorphological mapping, LiDAR imagery, boreholes and ERI surveys to characterize landslides in a Jurassic escarpment in the North York Moors (United Kingdom). LiDAR data served to assess the slope angle of particular zones. The authors showed how a multi-technique approach in a Lower to Middle Jurassic geological context provided a more general methodology for hazard assessments in a context similar to that of the VNCs.

The aim of this work was to define an approach combining photogrammetry with UAV and near-surface geophysical methods, which have never been carried out on this site. In the first section, the work gives a reminder of the VNCs site's geomorphology and geology. In the second section, aerial and geophysical measurements are presented. The adopted methodology is exposed and the technical details of the in situ implementation are specified. In the third section, a diachronic approach is tested over a 1-year period to assess erosion and accumulation of landslide volumes, and set the inputs of a 4-year diachronic study based on a UAV survey. Near-surface geophysical prospection is performed to give insight into the materials involved in landslides. Finally, this mid-term study combining aerial and shallow surface methods is discussed and can be considered on a larger scale.

Studied site, geology and morphology

The VNCs are part of the Pays d'Auge plateau (Normandy, France). They form a 4-km-long coastline between Houlegate and Villers-sur-Mer (see Fig. 1), subject to erosion caused by hydrological processes from the plateau and by tides at the toe (Maquaire et al. 2013; Roulland et al. 2019). A noticeable aspect is the local geology, dating from the Cretaceous to Jurassic periods, precisely described for the entire plateau by (Hassen et al. 2021). These cliffs are distinguished by the originality of their outcropping geological layers and their complex, chaotic morphology resulting from subaerial continental and marine processes (see Fig. 2), leading to a landscape of badlands (Maquaire et al. 2013). Close to Villers-Sur-Mer, the geological formations shown in Fig. 3, are, from top to bottom:

- in the Albian stage, a grey marl (4–7 m). In this stage, springs occur, resulting from the Cenomanian aquifer present higher (at 100 m NGF) in the plateau (Elhaï 1963);
- in the Mid Orfordian stage (Lebrun and Courville 2013), Coral Rag (Mid Orfordian; 0.2–5 m), limestones of Trouville (6–8 m), where main rocks sliding occur, clay of Lopha Gregarea and limestone of Auberville (18–15 m), where the main flows occur, accelerating mudflows;
- in the Lower Oxfordian stage, Ferrugineous oolite and marl of Villers, where crests and steep talwegs (gullies) characterize the badlands.

In order to better illustrate the morphodynamic characteristics of the VNCs, Fig. 4 taken from (Medjkane et al. 2018) shows how rock falls and mudflows shape the badlands formation.

Fig. 1 Aerial view of the whole 4-km-long VNCs between Houlgate and Villers-sur-Mer (Normandy, France, white-dotted rectangle). VNC case study is encircled in white rectangle (Image from ©IGN inside ©QGIS)

Former works have assessed the VNCs coastline's retreat based on visual inspection and literature: 0.15 $cm/year$over a period of 253 years according to (Maquaire et al. 2013), while (Quinejure 1971) gave 10m by 3 years to 40 cma day during major events and in particular locations. (Roulland et al. 2019, 2021) recently reported on an extensive study of the VNCs site's coastal erosion, based on (1) a complete historical gathering (from 1759 to 2016) of various maps and photos, (2) LiDAR data, and (3) meteorological events. Firstly, this work underlined the fact that the coastline defined as the limit between the plateau and the main scarp is retreating, by a distance ranging from −0.06 to −0.8$m/year$, depending on the coastal section considered. Secondly, the shoreline defined as the limit between the basal scarp and the beach is evolving slowly during the considered periods. Mudflows and rocks debris, as well as occasional major slidings (Maquaire et al. 2013), continuously fill the basal scarp, while tides, reinforced by strong events such as storms, take away offshore materials.

In order to complement all the VNCs results of the aforementioned studies, we aim to further the understanding of these

Fig. 2 **a** Clues of future rotational slidings at the main scarp surface (up to 70 m height), involving limestone rockfalls underneath Coral Rag. **b** Leakages that take their source at the grey marl Cenovanian top layer, triggering mud and rock slidings forming the basal scarp at the VNCs toe. **c** Housing threatened at the top. Pebbles, fossils and limestone blocks lean on the beach after tidal cycles accelerated by high-tidal events and storms. The biggest blocks are turning into black rocks covered by algae and mussels, and appear as black cows (in French: *vaches noires*) to sailors offshore

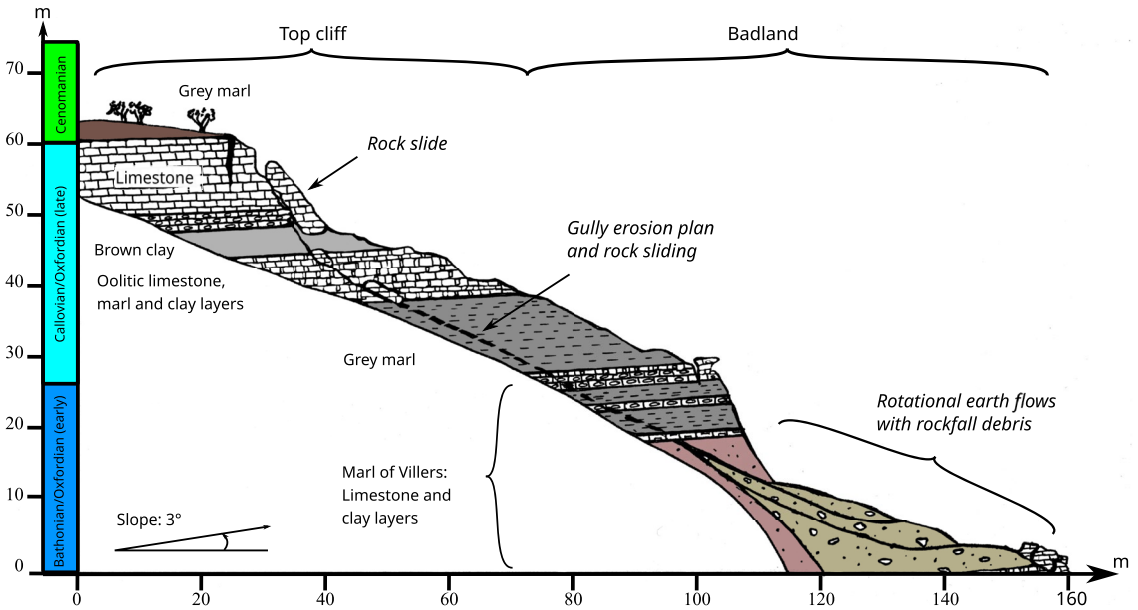

Fig. 3 Local geology of the badlands VNC in Villers-sur-Mer (Normandy, France). A first water table is known to exist between both limestones layers in the Callovian formation (45–50 m). Water flows are also in situ observed underneath the Cenomanian layer as well as between the Oolitic limestone and grey marl (redrawn from (Quinejure 1971)

erosion processes by carrying out a survey combining aerial and terrestrial geophysical methods, thereby establishing the basis for future research in the hydrogeological, geophysical and morphological domains.

Methodology

The combination of aerial and terrestrial exploration methods, enhanced with morphodynamic and geological data, is the proposed methodology to study how erosion and deposition evolve, and to determine the materials involved. We focus on a part of the VNCs, as depicted in Fig. 1 which represents a $300 * 300\ m^2$ area. The local topography, typical of badlands, is made up of deep ravines and steep crests shaping the front relief. Secondary and minor scarps are partly invisible from the beach. Many blocks of various sizes locally hide the topography leading to an occlusion phenomena and, as a result, an incorrect DEM assessment with TLS and terrestrial SfM. UAVs represent the ideal solution since photos are taken from the air. Assessing VNCs erosion and deposition volumes can provide answers to the coastal retreat. At least two DEMs are required.

This methodology was tested and validated during a 1-year period of observation, between April 2016 and April 2017, taking into account drone flights 1 year apart. Electrical

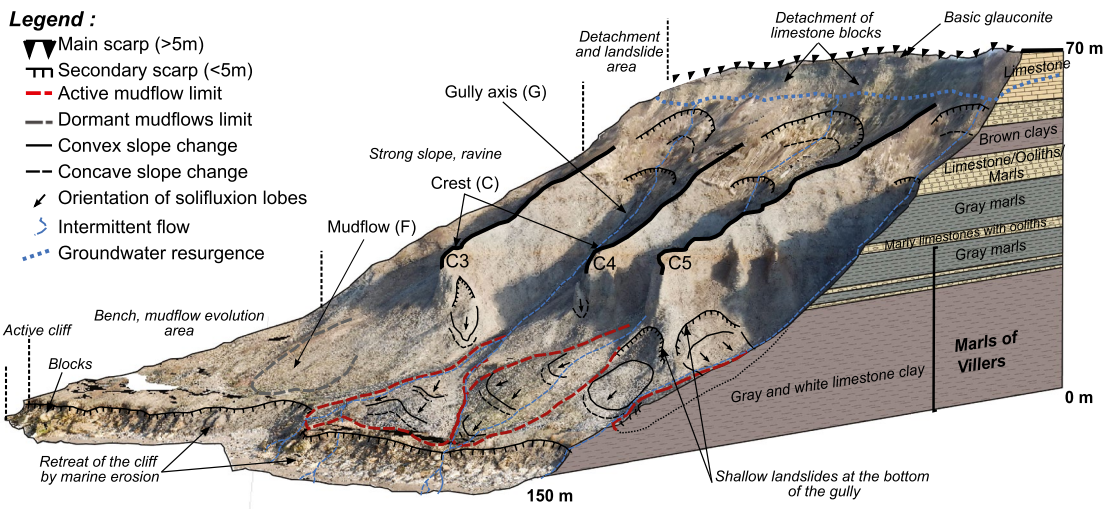

Fig. 4 Local geology in perspective with the 3D DEM model taken from (Medjkane et al. 2018) and morphodynamic interpretation

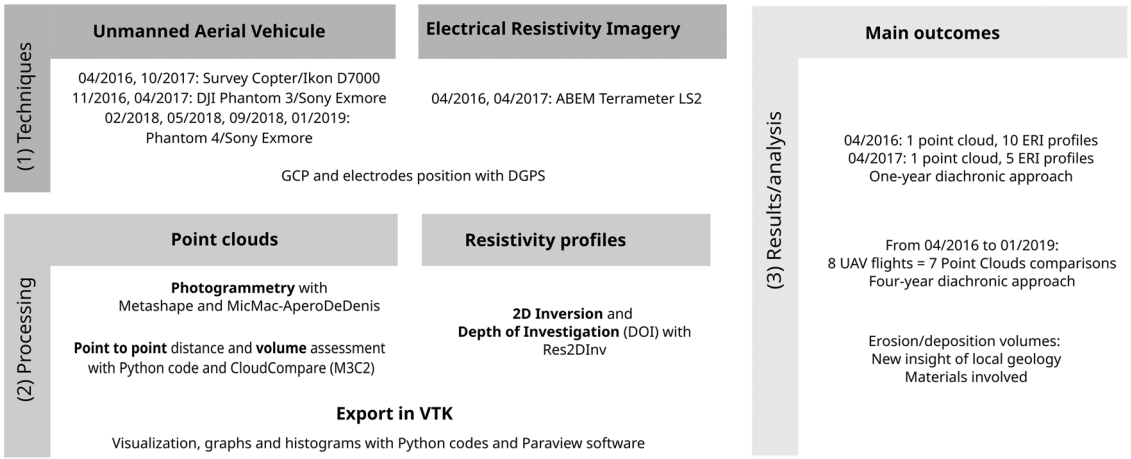

Fig. 5 Global methodology performed on the VNCs including (1) used techniques, (2) processing and (3) results and analysis

measurements were carried out at the same time as these flights with the aim of identifying the materials involved in the erosion and deposition phenomena. Finally, the rainfall was also recorded in order to study the difference between rainy events and mudslides or collapses observed between flights. The location of all ERI profiles as well as the UAV flight planning are shown in Fig. 6

For this purpose, UAVs equipped with cameras were used to build point clouds using both commercial Metashape software and the freeware code MicMac/InterfaceCEREMA (https://github.com/micmacIGN/InterfaceCEREMA). DEMs were obtained thanks to the CloudCompare freeware (version 2.10.2, [GPL software]. (2019). Retrieved from http://www.cloudcompare.org/. See, for example, (Stumpf et al. 2015). Morphodynamic areas similar to (Medjkane

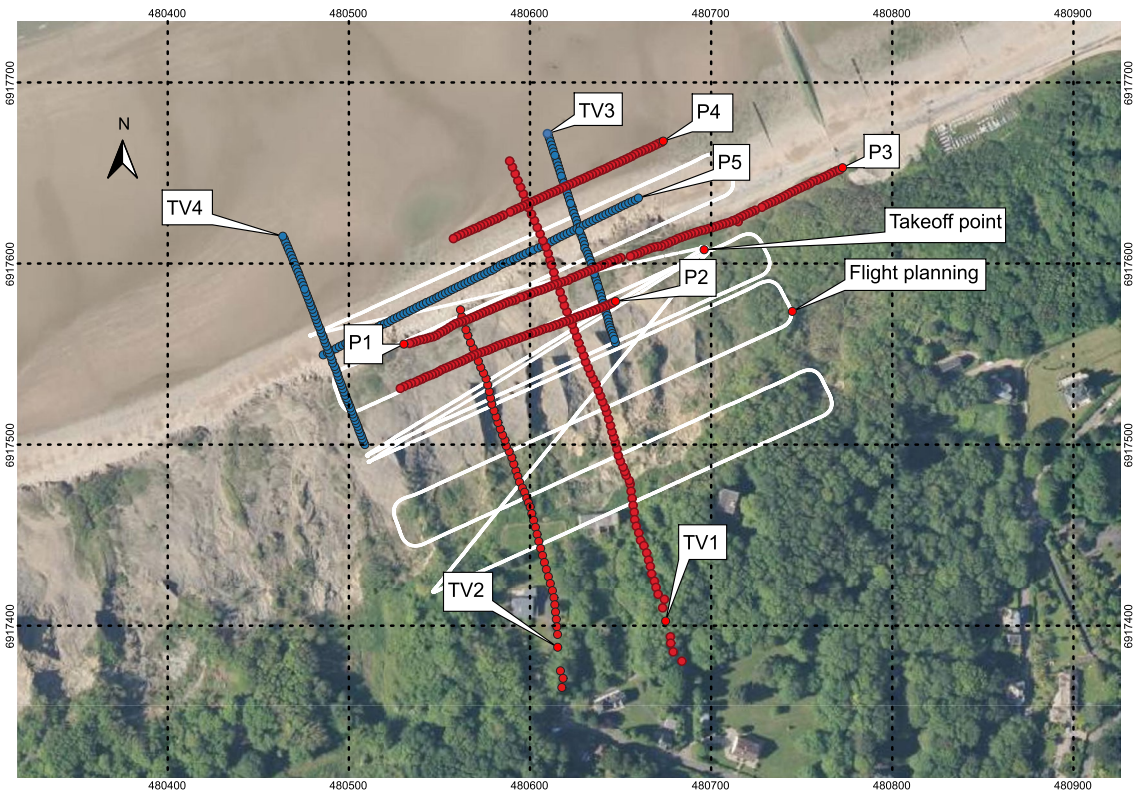

Fig. 6 Electrodes location of ERI profiles of (i) April 2016 in blue dots (transverse profiles TV1 and TV2, parallel profiles P1 to P4) and (ii) April 2017 in red dots (transverse profiles TV3 and TV4, parallel profile P5). The takeoff point of the drone is indicated as well as the corresponding flight planning in white line

et al. 2018; Roulland et al. 2019) were defined. They also provided TLS and SfM point clouds collected from the beach and carried out on the same UAV flight date, in order to compare the three approaches. A Python code was developed to process photogrammetric, TLS and SfM point clouds using CloudCompare, leading to a volume assessment inside each morphodynamic area.

The ERI was the only suitable geophysical method carried out in the VNCs site. Basically, it consists of injecting current with two electrodes into the near surface and measuring the electric potential with two other electrodes in the vicinity of the current flow. This operation is repeated with several electrodes alongside a profile (2D) and gives an array of current and potential with which the apparent resistivity of materials is calculated. The topography of the shallow surface is obtained with inversion: A model with finite-difference of the subsoil is built to compute calculated potentials and compared with the measured ones until the difference between their values is minimal. In this study, ERI inversion was performed using the Res2DInv software (Program Version 4.8.01. Copyright Geotomo Software. www.geoelectrical.com) (i) to describe the materials involved in the erosion process, (ii) to specify the local geology, and especially (iii) to assess the thickness of the deposits at the toe of the crests and on the basal scarp. The topography alongside the profiles was also taken into account for the ERI interpretation, thanks to GNSS measurements of electrode positions. A Terrameter LS2 system (Copyright ABEM) was used for the measurements. The need to study the whole cliffs led to a complex implementation in the field, combining ERI profiles with Wenner and Dipole-Dipole configurations, from top to bottom, and alongside the toe of the crests and on the beach. All characteristics of ERI profiles are given in Table 1 and are discussed in the following section.

All data (Point clouds, DEMs, calculated maps of erosion/deposition volumes and inverted electrical profiles) was exported in Visualization Toll Kit (VTK) format and combined using freeware Paraview (Ayachit 2015). The global methodology adopted in this work is shown in Fig. 5.

Finally, these first results and the methodology served to define a protocol of UAV monitoring and data processing that would be applied during the 4-year experiment from April 2016 to January 2019, including the outcomes of eight UAV flights. Unfortunately, electrical measurements could not be performed for drone flights after April 2017. For the first flight in April 2016 and the second flight in April 2017, a petrol engine drone (SurveyCopter) and an electric drone (Phantom 3 Pro by DJI) were respectively used to survey the same area. Other flights during the 4-year period were carried out using the same drone in alternation with a DJI Phantom 4 drone. Each drone carried a visible camera; all technical details concerning the three cameras and the eight flights are given in Table 2.

Results

Erosion and deposition volumes: 1-year flight testing

In this subsection, the erosion and deposition volumes are assessed between April 2016 and April 2017. The area studied covers around 90, 000 m^2. UAV flights in April 2016 and April 2017 followed a plan at respective heights of 150 m and 110 m, ensuring a surface coverage of 80 %between two images. 20 DGNSS-positioned GCPs are distributed as homogeneously as possible on the site. A photogrammetric

Table 1 Characteristics of the ERI profiles shown in Fig. 6, carried out in Dipole-Dipole (DD) and Wenner (W) configuration (*Quad.*: quadripole; *Stacking error at 1%*: variation coefficient of 1% between two measurements; *Err.*: root mean square error after a given number of itération (*Nb it.*) of the L1-norm inversion)

Name	Init. nb. of quad.	Final no. of quad.	Stacking Err. at 1%	Nb. elec.	Length (m)	Spacing (m)	Nb it. (L1-Norm)	Err (%).
P1-DD	888	888	2	64	126	2	7	1.5
P1-W	555	555	2	64	126	2	7	0.46
P2-DD	888	888	2	64	126	2	7	1.1
P2-W	555	555	2	64	126	2	7	0.98
P3	555	555	2	64	126	2	7	0.61
P4	555	555	2	64	126	2	7	0.43
P5-DD	1776	1771	2	96	190	2	7	1.6
P5-W	1110	1107	2	96	190	2	7	0.79
TV1-DD	1776	1758	2	80	316	4	7	4.3
TV1-W	1110	1110	2	80	316	4	7	0.71
TV2-DD	888	798	2	59	232	4	7	3.3
TV2-W	555	480	2	59	232	4	7	0.78
TV3	555	553	2	64	126	2	6	0.64
TV4-DD	888	888	2	64	126	2	7	1.1
TV4-W	555	554	2	64	126	2	6	0.83

Table 2 Characteristics of the UAVs and cameras used from April 2016 to January 2019

UAV	SurveyCopter	Phantom 3	Phantom 4
Flight	04/2016, 10/2017	11/2016, 04/2017	02/2018, 05/2018, 9/2018, 01/2019
Camera	Ikon D7000	Sony Exmor camera	Sony Exmor camera
Dim. (Px)	4928*3264	4000*3000	5472*3648
Focal Dist. (mm)	28	3.6	8.8
Pixel pitch (μm)	8.42	1.18	2.4
Flight height (m)	150	110	110
Pixel size (cm)	4.8	3.61	3
Image size (m)	237.1*157	144.2*108.2	164.2*109.4

construction of the DEM was performed thanks to the dedicated photogrammetric Metashape software and the MicMac freeware solutions. There were no significant differences (less than 3–4 cm for the target coordinates) between both software solutions, as reported by (Jaud et al. 2016). Approximately 100 photos were used to build both 3D point clouds. In Fig. 7a, b, the 2016 and 2017 3D point clouds are represented in the front view. They respectively contain 20,633,170 and 18,105,932 points (*pts*). The point density (pts/m^2) is calculated around core points of 1 m^2 and is 497 ± 59 and 456 ± 80, respectively. All data is georeferenced using the Lambert 93 coordinates system and translated to 480,000 m and 6,917,000 m in the x and y directions, respectively, in order to facilitate the graphical representation, and maintain significant data accuracy to correctly process the distance map using CloudCompare.

In Fig. 7c, the Multiscale Model-to-Model Cloud Comparison (M3C2, (Lague et al. 2013)module of CloudCompare is used to compute the point to point distance between 3D point clouds. The color scale is saturated to highlight the height variation between both point clouds. Areas of eroded volumes (in blue) are mainly located on the secondary scarp and in the gullies, while deposited volumes (in red) correspond to sand level variation on the beach and mainly to mudflow accumulation on the basal scarp. Firstly, while M3C2 processing serves to appreciate main morphodynamic behavior over a 1-year period, evaluating volumes requires the meshing of both point clouds using CloudCompare. Secondly, to assess the deposition and erosion volumes for a proper interpretation, the April 2016 morphodynamic shapes (area number and contour) similar to (Medjkane et al. 2018; Roulland 2019, 2021) are considered and represented in Fig. 8a.

- Area 1 is related to a part of the beach. Tides regularly move large volumes of sand, sediments and pebbles. Consequently, the level of the beach may well vary by several tens of centimeters depending on the power of the tide and on meteorological events. An accumulation of more than ≈ +950 m^3 is estimated between April 2016 and April 2017;
- Area 2 defines the basal scarp and the toe of the crests. Muds and limestone rocks accumulated, forming domed surfaces and representing a volume of about ≈ +700 m^3 between April 2016 and April 2017;
- Areas 3 to 8 correspond to gullies delimited by crests. Materials mainly eroded over the 1-year period in areas 3 to 7, corresponding to the steepest flanks of the cliffs and the most active zone subject to erosion from the plateau. Area 8 presents a lower slope compared with the other gullies, and corresponds to an area where erosion from the plateau is less active and vegetation can grow;
- Areas 9 to 14 represent the secondary scarp. The accumulated volumes in areas 9 and 10 correspond to limestone rockfalls, while erosion in areas 11 to 13 corresponds to limestone and mud swept away by water coming from the plateau.

Eroded and accumulated volumes using UAV photogrammetry are compared with TLS and SfM data (Medjkane et al. 2018) and the results are shown in Fig. 8b. Area 3 (active gully) shows significant differences between the three methods and remains to be interpreted. Area 8 is a partly vegetated gully with a very low slope where some occlusion phenomena occur in the SfM and TLS DEM. This remark is valid for the secondary scarp areas (9 to 11 and 13 to 14). TLS and UAV photogrammetry present a globally similar trend and tend to show that the TLS occlusion phenomena are less significant than the SfM one. Finally, Fig. 8c, d show the M3C2 positive and negative distance, respectively, and serve to identify the main eroded or accumulated areas between both UAV flights.

Electrical resistivity imaging

ERI profiles were carried out in April 2016 and in April 2017. All electrodes positions were controlled with DGNSS to take into account the topography. All inverted ERI data (see Figs. 9 and 10) are exported in VTK and displayed using Paraview software in the corresponding VNC 3D mesh (calculated with CloudCompare from both point clouds of April 2016 and April 2017). For each ERI profile, the theoretical depth of investigation (DOI) index is used to assess the confidence "below which the earth structure is no longer constrained by the data" (Oldenburg and Li 1999). This index is close to 0 if two inverted models give identical results, whatever the initial model values. The confidence limit is usually set between 0.1 to 0.2. In all the following results in this section, the DOI is displayed and discussed if needed. Finally, for Figs. 11, 12, and 13, the resistivity distribution is given to identify the resistivity of the main formations.

Concerning the longest transverse profiles of April 2016, namely TV1 and TV2, Dipole-Dipole (Fig. 9a) and Wenner (Fig. 9b) configurations were performed. A focus on the Dipole-Dipole configuration was chosen, since a rapid analysis shows that the local geology seems to be

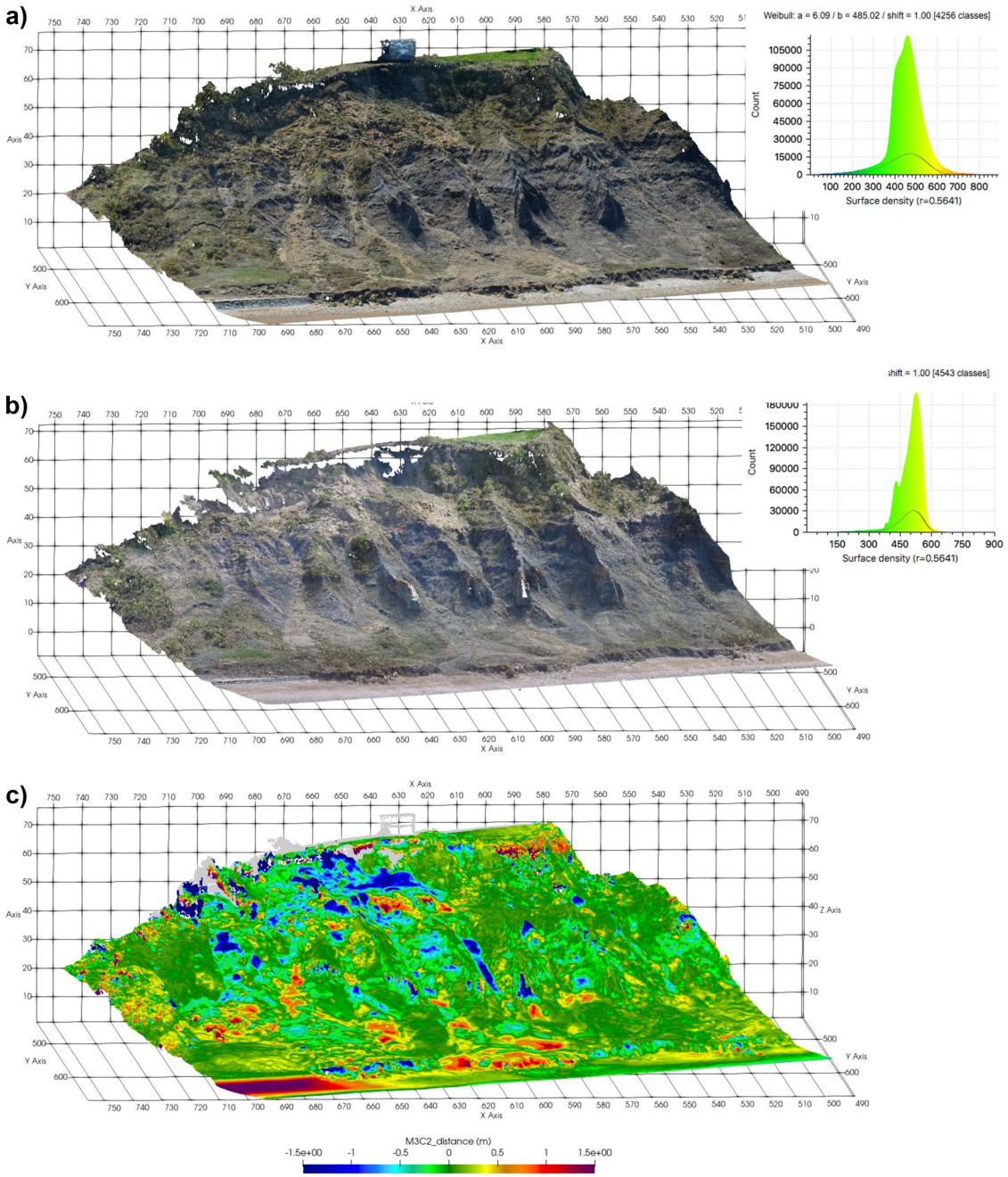

Fig. 7 **a** April 2016 and **b** April 2017 3D point clouds with corresponding histograms of point density (pts/m^2). **c**The distance calculated between the 2017 and 2016 3D point clouds with the M3C2 module (Lague et al. 2013) of CloudCompare (version 2.10.2, [GPL software]. (2019). Retrieved from http://www.cloudcompare.org/). The three views are displayed with Paraview (Ayachit 2015)

better described using this protocol. Accordingly, these two profiles are represented in a Dipole-Dipole configuration in Fig. 11 and start at the plateau (≈90 m long flat surface). As mentioned previously, TV1 ends on the beach while TV2 ends on the basal scarp, due to the tide level on the day of measurement. Both configurations clearly show:

- A first heterogeneous layer less than 10 m thick and corresponding to (see "Sect. 2" and Fig. 3a) the grey marl (Albian stage, $\rho_a \in [10;20]\ \Omega.m$) and the Coral Rag (Mid Orfordian stage, locally on TV2 $\rho_a \geq 100\ \Omega.m$) layers.
- A high resistive layer (limestone of Trouville, $\rho_a \in [50;250]\ \Omega.m$) forming a single block about 10 to 20 m thick in TV1 and the clay under which limestone of Auberville layers are partly visible, whereas the TV2 profile shows a global resistive block of more than 30 m in depth.

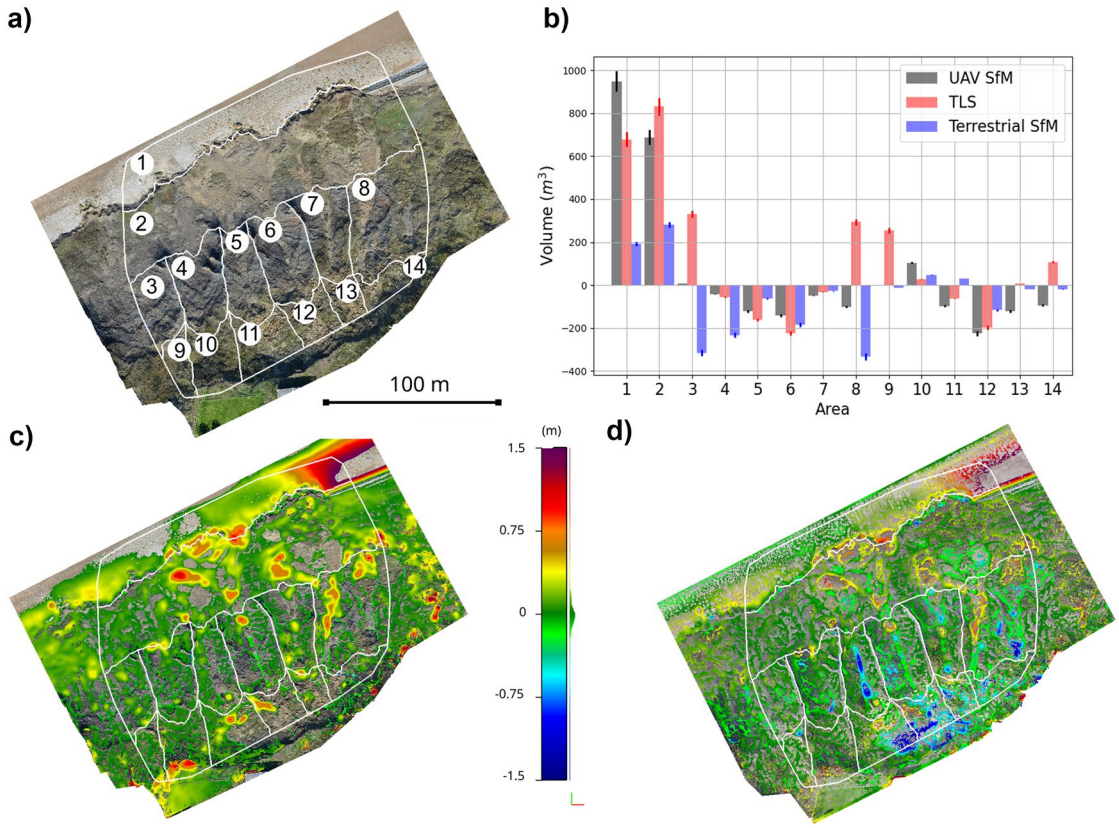

Fig. 8 **a**14 morphodynamic areas similar to (Medjkane et al. 2018; Roulland et al. 2019, 2021). Area 1 is related to a part of the beach. Area 2 is the basal scarp surface. Areas 3 to 8 correspond to crests and gullies. Areas 9 to 14 correspond to the secondary scarp just underneath the plateau. In all these areas, the DEM is calculated and **b** erosion/deposition volumes (in m^3) are assessed between April 2016 and April 2017 and compared with TLS and SfM data collected on the same measurement dates. The M3C2 distance shows the main deposition and erosion surfaces appearing **c** above the April 2016 DEM and **d** beneath the April 2017 DEM

Dipole-Dipole and Wenner TV1 and TV2 profiles continue to the cliff slope where electrodes were placed at the limit between active flows in the gullies and slope crests (areas 4 and 5). Interpreting the Wenner configuration here is partly irrelevant: Fig. 9b vertical structures are depicted whereas the local geology is known to consist of horizontal layers. A focus in the discussion explains why (see "Sect. 5"). In Fig. 11a, the Dipole-Dipole configuration yields more interesting results, without clearly reproducing the multi-layered geology depicted in Fig. 3 and reproduced in Fig. 11b. Resistive and conductive areas are alternately detected at the second scarp, where debris from upper limestone of Trouville accumulates with clay and upper marl of Villers. A resistive to conductive layer (from 70 to 5 $\Omega.m$) at mid-slope may correspond to the erosion plane containing shallow rocky materials sliding from the secondary scarp, covering a marl layer sub-base.

From the toe of the crests to the basal scarp, ERI data show a ≈ 10 $\Omega.m$ shallow formation corresponding to accumulated materials (mainly marl and clay). Finally, from the basal scarp to the beach, the TV1 profile shows a low resistive layer (10 to 20 $\Omega.m$) at a depth of about 5 m, corresponding to the marl of Dives formation, covered by a very conductive sand layer (less than 5 $\Omega.m$) mixed with erosion deposits and salt water about 3 to 5 m thick.

For both profiles, the DOI shows that ERI results must be interpreted carefully as far as the deeper formation is concerned, at least at the plateau and at the cliff slope. Whatever the configuration, ERI results barely reflect the actual multilayered geology in the cliffs slope; however, this technique is more relevant at the plateau and on the beach.

ERI profiles in the Wenner configuration parallel to the shoreline, performed at the toe of the crests (P2), at the basal scarp (P1 and P3) and on the beach (P4) are displayed in Fig. 12. The accumulated materials (marl, clay and limestone blocks) at the toe of the crests (P2) represent a ≈5 m thick layer of ≈10 $\Omega.m$ overlaying a more resistive layer corresponding to the marl of Dives formation. Shallow and resistive anomalies corresponding to limestone blocks sliding from upper layers are located in the exact direction of the gullies. These resistive anomalies stretch laterally as the mudflows reach the basal scarp (P1). From P2 and P1, a first upper layer results from successive mudflows: resistive materials from the upper formation accumulate in the direction of the gullies, and clayey materials at the toe of the crests. Its thickness varies, and forms an irregular interface with the deeper formation (marl of Dives). The P3 profile shows a very resistive part (≈120 $\Omega.m$), corresponding to an inactive area (no mud, no sliding). Here, the marl of Dives formation (≈10 to 15 $\Omega.m$) is located at a depth of approximately 10 m. Finally, the P4 profile carried out on the beach at low tide clearly shows the ≈3 to 5 m thick sand layer (≈1.5 to 2 $\Omega.m$) saturated with salt water, covering the marl of Dives layer.

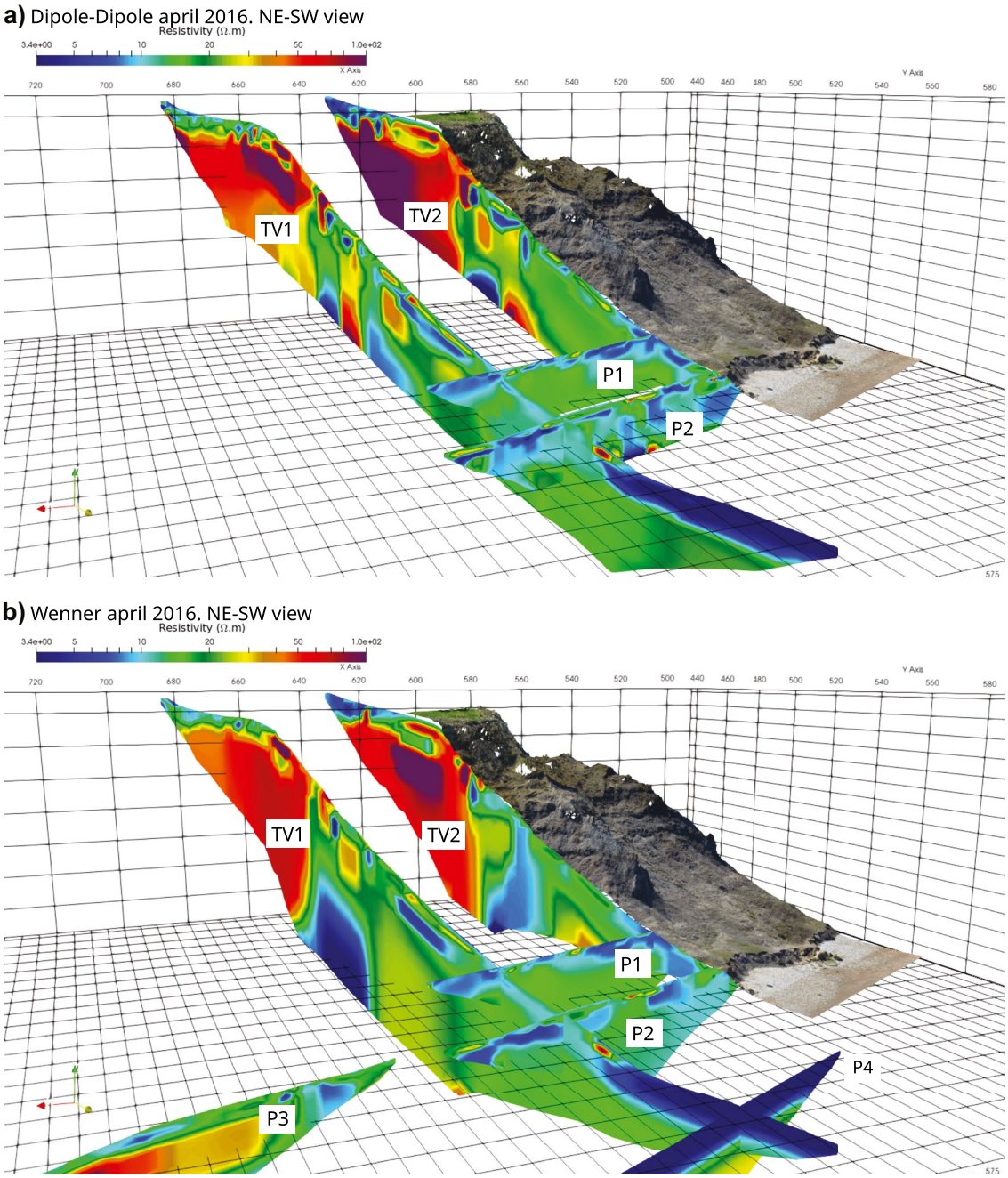

Fig. 9 Dipole-Dipole and Wenner electrical profiles of April 2016. Inverted resistivity profiles are shown in a cut point cloud of the VNCs recorded with a UAV in the corresponding year

The TV4 and P5 profiles shown in Fig. 13 were carried out in a Dipole-Dipole configuration in April 2017. The P5 profile parallel to the shoreline was performed on the beach at approximately 20 m from the basal scarp. Two main layers correspond to the sand (≈ 3 to 5 m thick) saturated with salt water and to the deeper formation of marl of Dives, respectively. Unlike the Wenner configuration (see Fig. 12), the interface is irregular since the Dipole-Dipole configuration is more sensitive to lateral variations (Loke and Barker 1996a). These variations may be related to a limestone accumulation now buried in the sand. It can also indicate that the top of the marl of Dives formation may be rough or partly fractured. To complement the interpretation of both the TV1 and TV2 Dipole-Dipole profiles of April 2016, the TV4 profile of April 2017 aims to precisely locate how the marl of Dives formation extends under the basal scarp. Surprisingly, as the sand's thickness narrows in the direction of the cliffs, the marl of Dives formation seems to sink under the basal scarp, revealing an intermediate layer (less than≈10 $\Omega.m$) that may correspond to (i) the marl of Villers formation as shown in Fig. 3 or (ii) old materials eroded and accumulated between

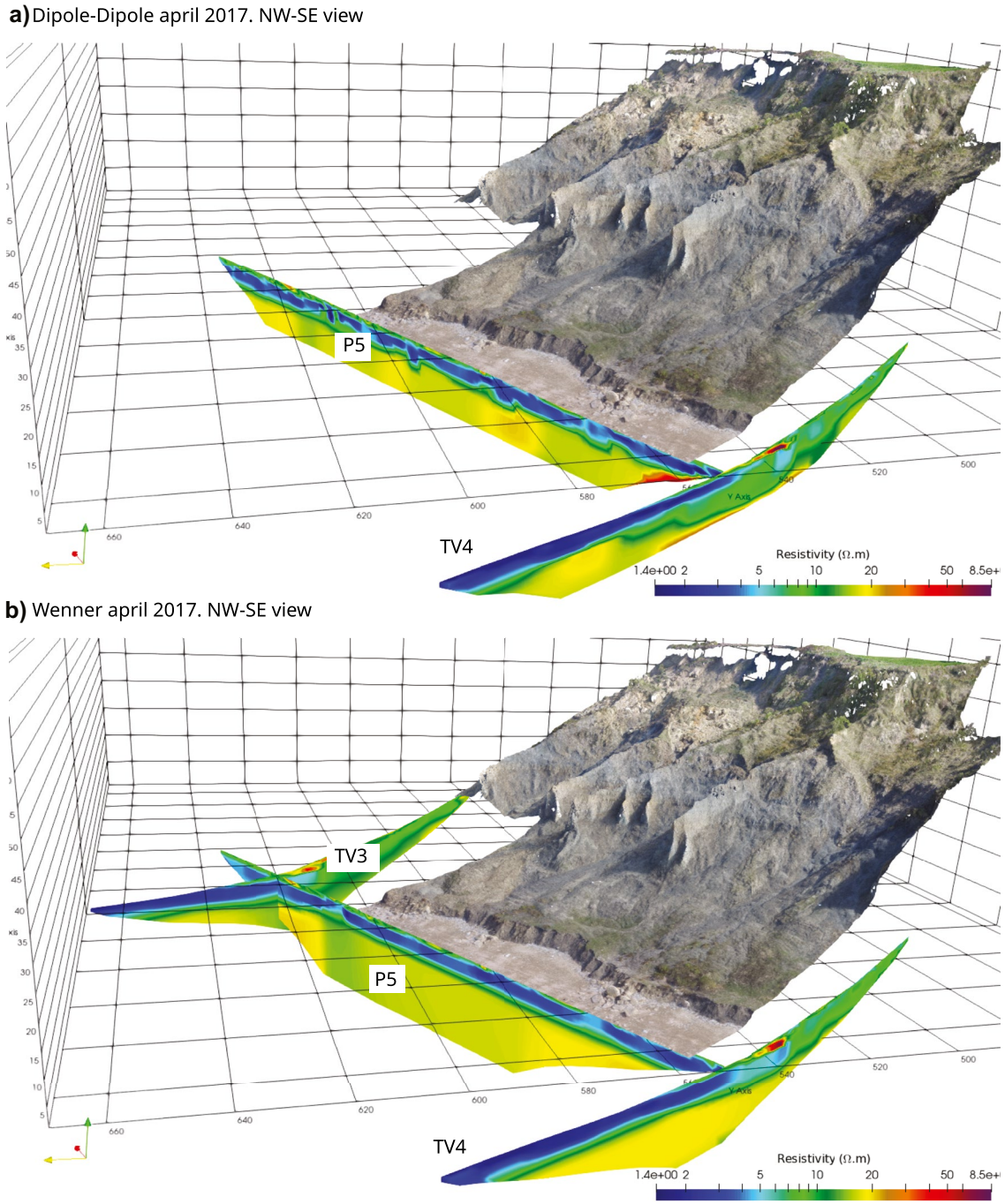

Fig. 10 Dipole-Dipole and Wenner electrical profiles of April 2017. Inverted resistivity profiles are shown in a cut point cloud of the VNCs recorded with a UAV in the corresponding year

the beach and the toe of the cliffs. As the profile extends to the clifftop, a shallow resistive anomaly appears at the beach/basal scarp transition and may be an artefact due to the strong variation in altitude (more than 50%between two electrodes, see (Loke and Barker 1996a). At the end of the profile, materials accumulated at the toe of the crests are visible; however, their thickness remains difficult to assess.

Erosion and deposition volumes: 4-year diachronic study

After validating the assessment of erosion and deposition volumes during the 1-year period by comparing two DEMs, the aim was to extend this approach to a 4-year period with eight DEMs, carried out between April 2016 and January 2019. In order to better explain this approach, Fig. 8a must be considered to recall the studied morphodynamic areas on which this section focuses. Figure 14

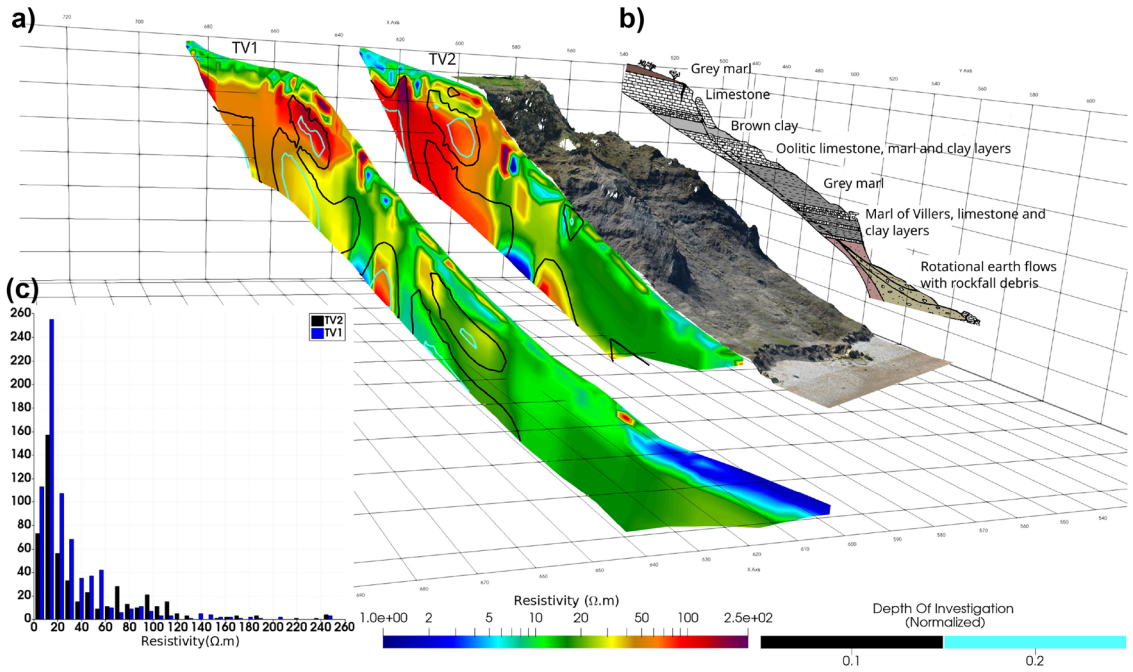

Fig. 11 **a** TV1 and TV2 Dipole-Dipole resistivity profiles and depth of investigation compared with **b** the local geology (Fig. 3a, c) Distribution of the main resistivity values of TV1 and TV2

summarizes the eight drone flights carried out during the 4-year period, and defines the number of the comparison between two consecutive DEMs (C-DEMs) as well as the average precipitation recorded near to the study site (Deauville station, available data at https://www.infoclimat.fr/). A C-DEM gives the volume difference calculated using the Metashape software. Figure 15 displays, in two dimensions, the results of the seven C-DEMs obtained for the eight drone flights during the 4-year period, for the 14 morphodynamic areas. Accumulated volumes (in red) and eroded volumes (in blue) are shown as a heatmap, and their values in m^3 are displayed in the corresponding cells. For the sake of clarity, on the top row, the types of main morphodynamic areas (beach, basal scarp, gullies and second scarp) corresponding to the area number (Fig. 8a) are recalled. Finally, the second to last row and the right-hand column give the sum of eroded and accumulated volumes during the 4-year period for each morphodynamic area and each C-DEM, respectively. These representations allow the following interpretation, considering the areas of Fig. 15.

- The beach and the basal scarp (areas 1 and 2) show the largest volume variations. In fact, these variations reflect different phenomena: tides, sometimes combined with storm episodes, can alternately carry materials offshore (C-DEMs 2 to 4 and 7), and bring sand and sediments on to the beach (C-DEMs 1, 5 and 6). On the basal scarp, materials (clay, marl and limestone) tend to accumulate and are then brutally swept away by strong meteorological events (C-DEMs 4 and 7);
- Over the 4-year period, a global erosion (≈ -1175 m^3) occurs in the gullies in areas 3 to 8. The height of ridges and flanks erodes with the rain, and materials continuously flow to the basal scarp. Area 8 alternates with erosion and deposition, but here the role of the vegetation should be considered. This area tends to retain materials (C-DEMs 3, 5 and 6) and sometimes collapses (C-DEMs 1, 4, 7);
- Materials of secondary scarp (areas 9 to 14) are mainly composed of limestone rock debris and may sometimes accumulate (area 10 and, to a lesser extent, areas 11, 13 and 14) or continually erode (area 12). The vegetation also can play a key role in the balance, particularly in areas 9, 10 and 14, and volumes may be overestimated. Nevertheless, materials including this vegetation end up being swept away to the gullies, and the overall balance over the 4-year period shows an active erosion (≈ -1500 m^3). All secondary scarp areas are in direct contact with the main water table visible on site, flowing from the plateau.

We will now consider the C-DEMs in Fig. 15, taking into account the precipitation over the 4-year period shown in Fig. 14:

- C-DEM 1 shows a global erosion in all areas except on the beach and the basal scarp where materials naturally accumulate. Nevertheless, it corresponds to eight months of normal precipitation and there is no obvious correlation between precipitation and erosion;
- Strong episodes of erosion can occur on all cliff areas (≈ -3600 m^3 and -3190 m^3 for C-DEMs 4 and 7, respectively), and erosion and accumulation can alternate in various areas, showing a global accumulation (≈ +960 m^3, +1510 m^3 and +1220 m^3 for C-DEMs 3, 5 and 6) or a global erosion (≈ -370 m^3 for C-DEM 2);
- C-DEM 3 mainly shows accumulation on all areas (except on area 12 and on the beach) after a normal level of precipitation, ended by a strong level in September 2017 (more than 175 mm). It seems that this event did not trigger any mudflows or rock

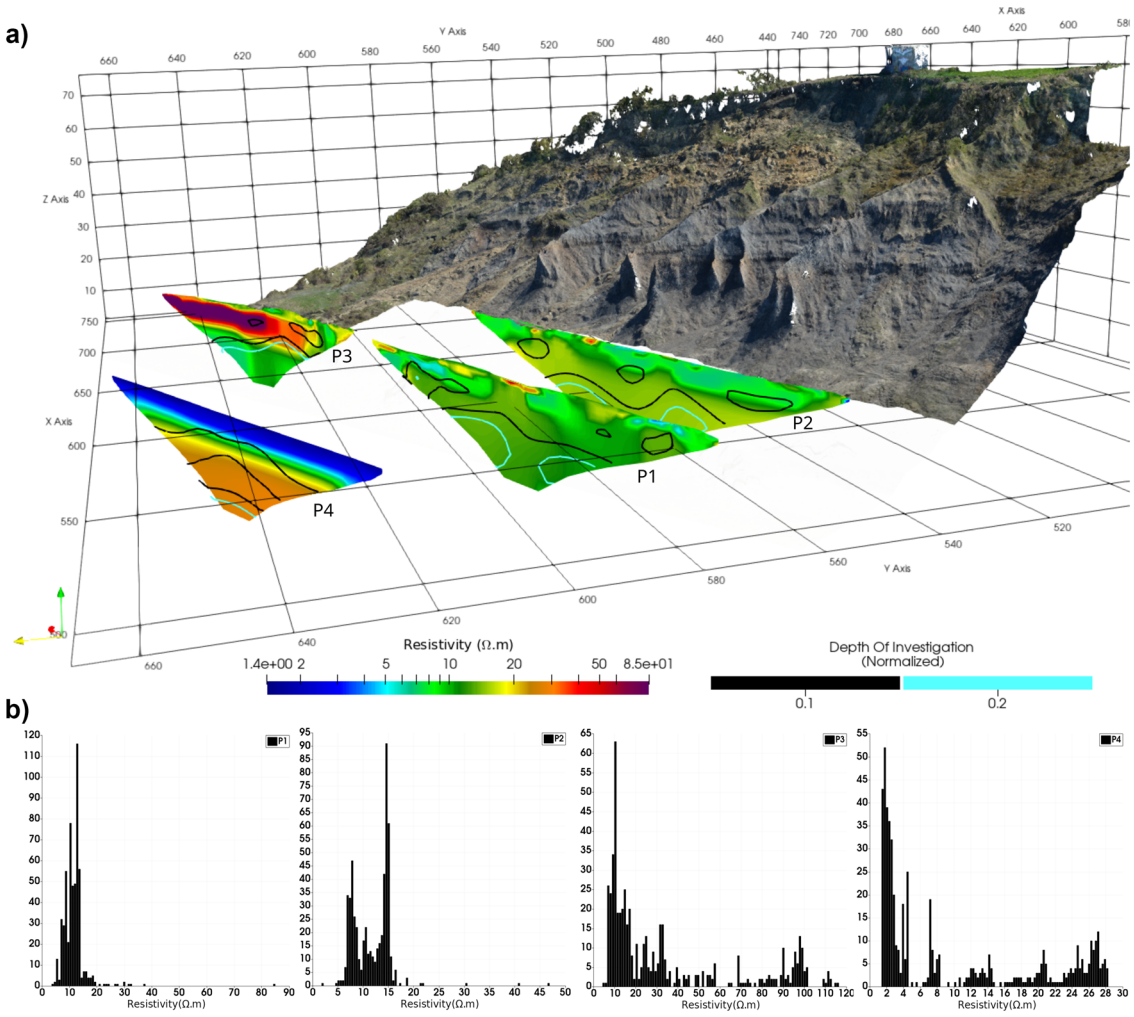

Fig. 12 **a** Wenner ERI profiles at basal scarp (P1, P2 and P3) and on the beach (P4), April 2016 and, **b** distribution of their main resistivity values

slidings. This remark is true for every C-DEM, indicating again that the erosion process and precipitation are not necessarily time-correlated.

Discussion

The UAV survey over a 1-year period enables the assessment of volumes of eroded and accumulated materials. The DEM built with 3D point clouds thanks to aerial drone flights avoids the occlusion phenomena inherent in the terrestrial methods (TLS and terrestrial SfM). The error associated with calculated volumes remains difficult to assess. Firstly, vegetation can differ from one flight to the next in some areas: in the present simple approach, no processing was applied to remove vegetation from the DEM. In future, this can be performed using tools such as the CloudCompare CANUPO (Brodu and Lague 2012) software, based on the classification algorithm. Fortunately, for this 1-year study, most of the areas considered are devoid of vegetation, except areas 8 and 10, as seen in Fig. 7 between X∈ [580;595 *m*] where the red area corresponds to vegetation growing between April 2016 and April 2017. Secondly, even if aerial photos yield more comprehensive 3D points clouds, hidden zones still exist when the topography is complex, as is the case in this badlands context: for instance, the shape of 3D rocks cannot be perfectly reproduced since some parts may be concave regarding the UAV position. Moreover, where the topography varies considerably, i.e., at the main scarp and at the toe of the crests, some points are missing in both the April 2016 and April 2017 DEMs (see Fig. 7). In conclusion, the margin of volume estimation error using the photogrammetric method is about 2%, according to similar experiments such as (Raeva et al. 2016).

ERI is the most widely used method in a badlands context (Perrone 2014)since it is sensitive to a wide range of resistivity (Telford 1990). The efficiency is low: for example, TV1 and TV2 require one day-long survey with five people, P1, P4, P5, TV3 and TV4 profiles, two days. ERI serves to identify main and shallow geological formations, and the Wenner and Dipole-Dipole configurations are complementary: the first is suitable for imaging vertical changes of resistivity, while the second is more sensitive to lateral changes (Loke and Barker 1996a, b). Nevertheless, neither configuration is satisfactory for imaging multilayered geology in the slope section: as depicted in Fig.15, ERI results from the first scarp to the toe of the crests show deep vertical zones while the local geology layers are virtually horizontal.

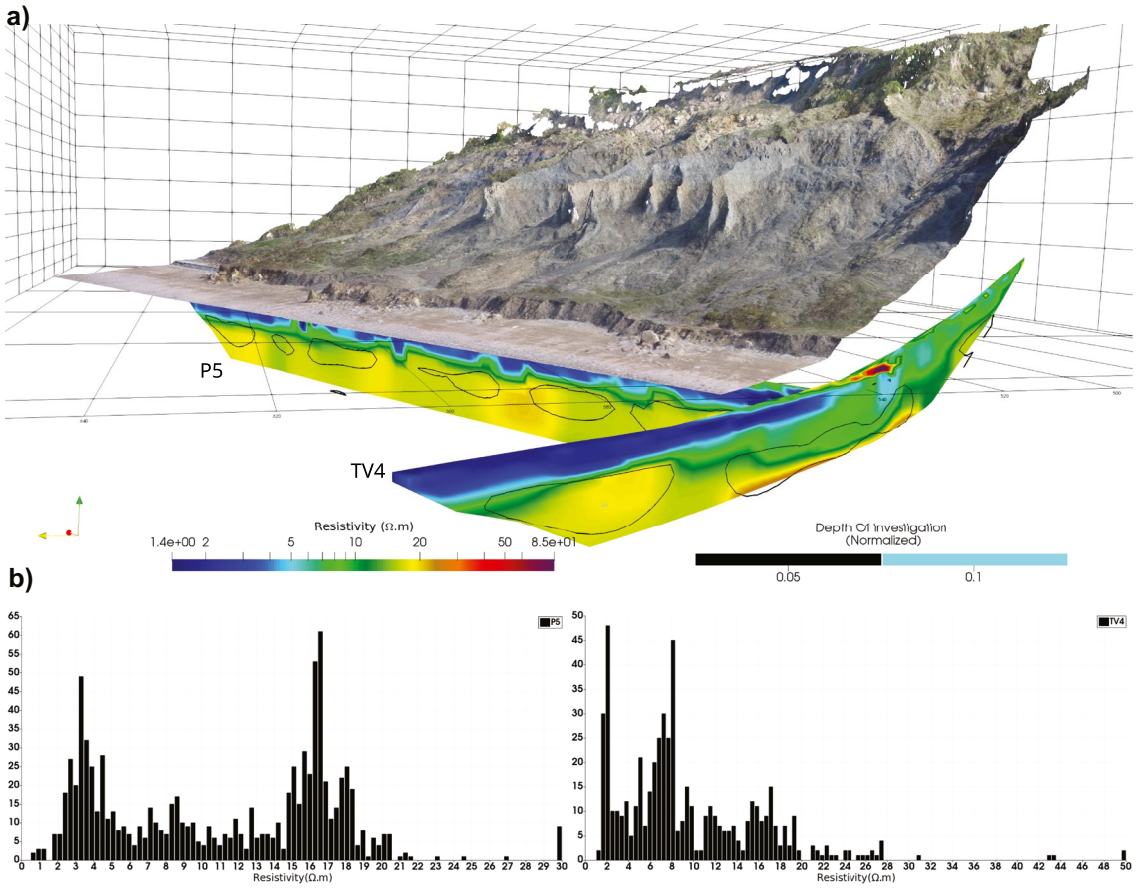

Fig. 13 **a** TV4 and P5 profiles carried out in April 2017 and **b** distribution of their main resistivity values

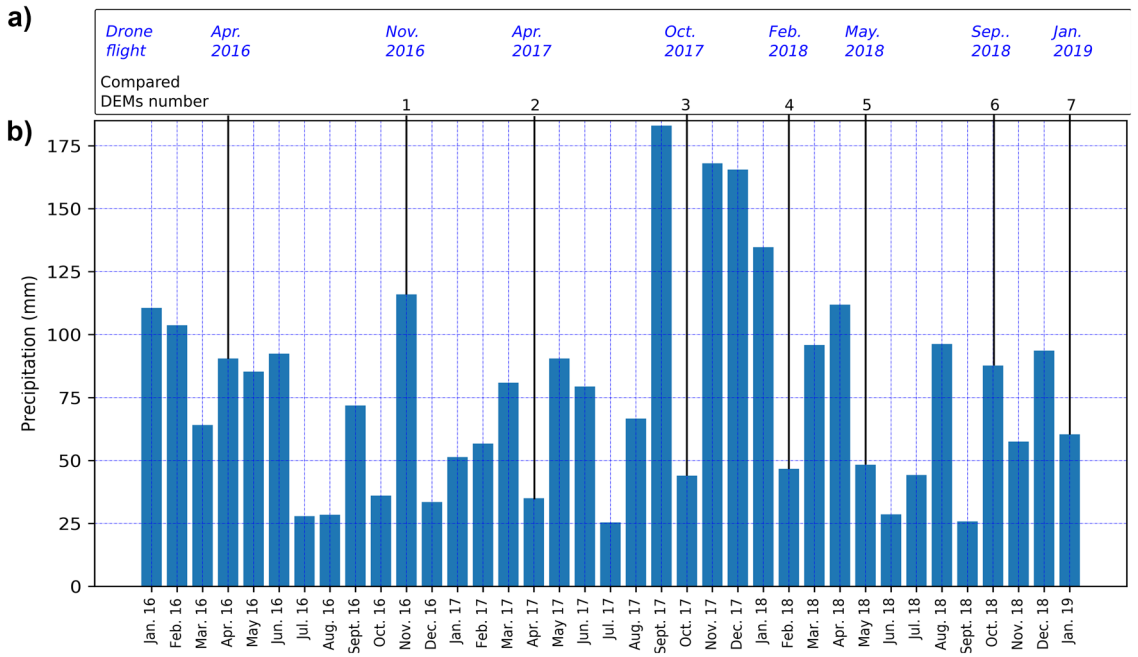

Fig. 14 **a** Dates of eight drone flights from April 2016 to January 2019 and corresponding to C-DEM. **b** Precipitation at the nearest meteorological station over the same period: data provided by https://www.infoclimat.fr/ at Deauville (France)

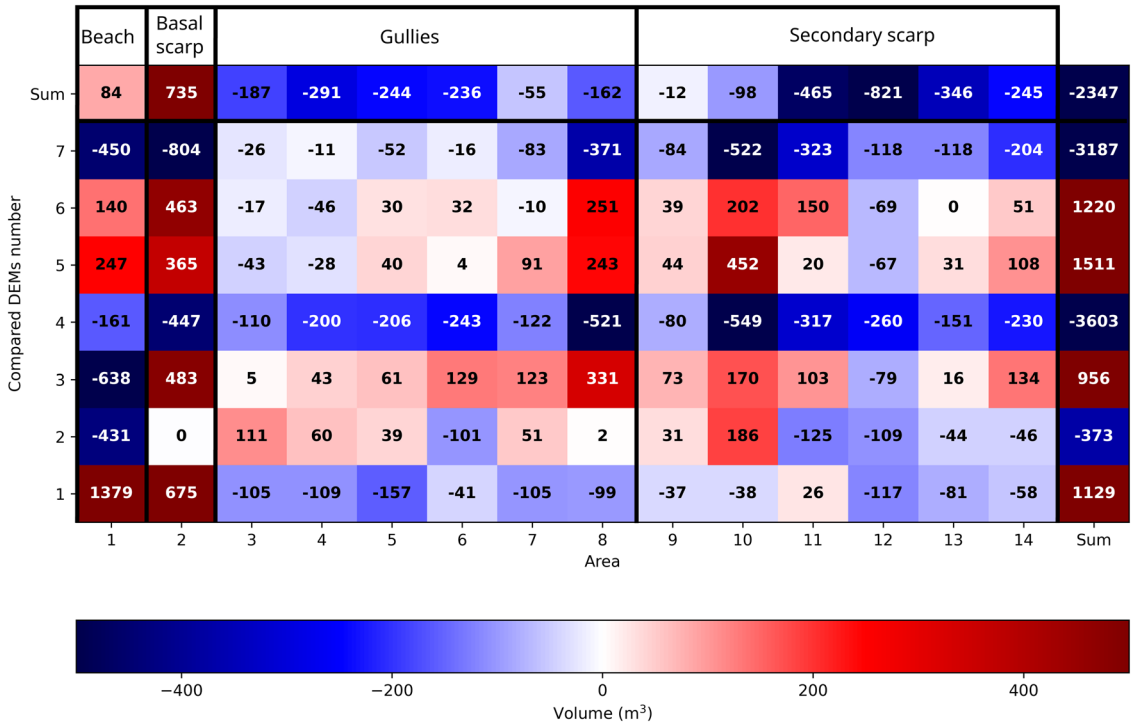

Fig. 15 Heatmap of the accumulated (red) and eroded (blue) volumes on the 14 morphodynamic areas defined in Fig. 8a and for the seven pairs of consecutive DEMs corresponding to the eight drone flights between April 2016 and January 2019. The second-to-last row and the right-hand column are the sum of eroded/accumulated volumes for each area and each DEM comparison, respectively

The DOI index as defined by (Oldenburg 1999)offers a qualitative interpretation of inverted apparent resistivity, and the results lead to a limitation of the method: all ERI results show a limited DOI close to the sides of inverted profiles. Moreover, the 0.1 limit is deepest where the resistivity value is low, while the method is limited on a more resistive medium (like limestone formation) (Loke and Barker 1996a). Such phenomena have been particularly well described in (Marescot 2008): the current flow is reduced in resistive zones, and the information is consequently less, as depicted in Fig.9 on TV1 and TV2 profiles from the plateau to mid-slope.

These first ERI measurements lead to the definition of an enhanced methodology for future experiments: other configurations should be relevant for mapping both horizontal and vertical changes of resistivity, such as the Wenner-Schlumberger configuration, which may increase the yield while improving quality (Loke and Barker 1996a). ERI also shows a limited efficiency in terms of describing the multilayered geology alongside the cliffs slope. Firstly, a priori information should include the location of layers visible in the field as well as the 3%-slope of the geological layers (see Fig. 3). (Zhou 2014; Zhou 2016)proposed an original inversion method considering the available structural information; this approach should be taken into account in future research. Moreover, it is obvious that the classic 2D inversion provided by the Res2DInv software is limited for a complex topography such as that in the badland context: all transverse profiles should be inverted by considering the steep crests and scarps in three dimensions. For this purpose, software such as pyGIMLi (Günther et al. 2006; Rücker 2006; Rücker et al. 2017)has shown reliable results in complex coastal environments (Udphuay 2011)and will be considered in the future. Finally, ERI can also be implemented for long-term monitoring to better identify the hydrological phenomena involved in the erosion process and landslide (Palis 2017), and the topography recorded by aerial means (included UAV) combined with a 3D inversion approach and a supplementary analysis of soil (Boyd 2021; Huntley 2019; Merritt 2014) would no doubt lead to an enhanced interpretation. Such an approach will be considered in future works.

The 4-year survey is the first diachronic study carried out using UAVs on the VNC. While similar experiments have already been presented for landslide phenomena (see, for instance, the Slovenian case study of (Peternel 2017), this is the first time a DYNALIT site in a badlands coastal context has been studied in this way: erosion and deposition volumes are assessed approximately twice a year. A general methodology has been defined based on free software applications and tools, allowing this assessment to continue over a long time period. It can also be extended to the whole 4-km-long VNC coastline, where other similar sites present the same badlands facies facing the sea. A numerical evaluation of the volumes is proposed depending on the morphodynamic shape, proving that active erosion ($\approx 3160\ m^3$ during the 4-year period) takes place in the gullies and the secondary scarp, while materials continually accumulate on the beach and the basal scarp, sometimes counterbalanced by brutal erosion events. This approach also underlines massive erosion periods ($\approx 3600\ m^3$ and $3200\ m^3$for C-DEMs 4 and 7, respectively) as well as periods where accumulation and erosion can alternate on morphodynamic areas. Finally, this 4-year study serves to identify the most active erosion areas: gullies 3 to 6, directly connected to the upper secondary scarp areas 9 to 12, corresponding to the flow of resurgent water from the plateau's most active water table

(Hassen 2021). In addition, the role of precipitation will need to be further investigated. Indeed, there is no concomitance between heavy rainfall and erosion phenomena. The saturation of the clay materials that generate the mudflows depends on both the rate of precipitation and the water circulation conditions within the formation. Consequently, the activation time of the erosion phenomena remains very difficult to evaluate.

The main question that remains to be answered is how often UAV flights should be carried out. Indeed, between two drone flights, materials may have been eroded and washed out to sea. This is particularly true for clayey and marly materials at the basal scarp or on the beach, while massive blocks of limestone tend to stay longer. Finally the volume assessment at the junction between the beach and the basal scarp, and on the beach itself, is only indicative. It does not reflect how much material has accumulated or eroded given the daily action of the tide cycle together with a virtually continuous flow of materials coming from the cliffs. Nevertheless, the UAV volume assessment provides an interesting observation: at the main scarp, rock fall and sliding are clearly identified, and the distance of the cliffs' retreat is about 1 m during the 4-year period (see, for example, Fig. 7 at around $X = 610m$). This quantification at the main scarp has recently been confirmed by (Roulland et al. 2021).

These measurements, carried out using a drone and the ERI method, serve to evaluate the evolution of the volumes of materials over a given period, and to image geological formations involved in the erosion of the VNCs. Presently, the objective is to further the analysis based on the link between hydrogeological processes coming from the plateau and activating erosion processes. A recent work (Hassen et al. 2021)proposed a 3D geological modeling that helps to understand how and where groundwater erodes materials, and what the total volume subject to erosion along the 4-km-long VNCs would be. Other methods would be suitable to detect preferential flows such as the spontaneous potential (Jouniaux et al. 2009). Seismic methods used in a similar context (Grandjean 2011; Fressard 2016) can also offer interesting results in these multilayered contexts. Finally, geotechnical tests are missing, and may have to be considered in the near future to properly calibrate geophysical results, despite the harsh access conditions in this badland context.

Conclusion

UAV and ERI measurements were carried out between April 2016 and January 2019 on the VNCs (300 m long, 300 m wide, 70 m high), an area that is part of a 4-km stretch of badland coastal cliffs subject to strong erosion. This is the first 4-year study performed on this DYNALIT site using these methods. The main objective was to define a methodology that would allow the assessment of the eroded and accumulated volumes of materials. A first diachronic approach was proposed, consisting of two UAV flights 1 year apart. Two DEMs of the VNCs were obtained. A zoning scheme led to a definition of the morphodynamic areas, where eroded and accumulated volumes were estimated. This approach was finally adopted for a 4-year diachronic study, based on eight DEMs, representing approximately two flights a year. The global erosion of the VNCs was quantified. The ERI method was performed to image the materials involved in the erosion process. From the top to bottom of the cliffs, ERI profiles provided information available at the plateau and from the basal scarp to the beach, by identifying the main layers of the local geology that contribute to the erosion and accumulation process. Profiles parallel to the shoreline yielded an estimation of the material thickness at the toe of the crests and on the beach. ERI based on classic 2D inversion and without a priori information was partly irrelevant between crests, due to the strong topographical badland context. All these measurements form the basis of future research that will be conducted as part of a new project recently funded by the Normandy Region.

Acknowledgements

The authors thank the council of Villers-Sur-Mer for granting permission to conduct surveys on a protected area. We gratefully acknowledge Jean-Luc Sorin of the University of Gustave Eiffel who performed the first UAV flight in 2016 and another in 2017.

Author contribution

Cyrille Fauchard managed the Regional TéléDéTAC project, wrote the full article and managed the processing flow. Vincent Guilbert ensured optimal on-site data measurements, data consistency between the software solutions used, and performed several tests to provide the best inverted ERI and DOI data using Res2DInv. He implemented the Python code to carry out the volume assessment of each VNCs morphogeological area between C-DEMs. Raphaël Antoine contributed to the discussion section and ensured two drone flights. Cyril Ledun managed the construction of some DEMs using the Metashape and MicMac software solutions. Bruno Beaucamp performed four UAV flights and built the QGIS maps of the articles. Stéphane Costa and Olivier Maquaire provided the main historical, morphogeological and geological data. Mohand Medjkane and Thomas Roulland shared their TLS and SfM data and graphical results. Robert Davidson ensured the DGNNS measurements. All authors participated in the measurements in the field.

Funding

This work was funded by the Normandy Region in the context of the TéléDéTAC (TéléDétection par drone du TrAit de Côte, 2017-2020) project. The Normandy Region recently decided to pursue this research as part of a new 2022-2025 project. This research has also benefited from the support of the Cerema, the University of Caen Normandy, and the University of Rouen Normandy.

Data availability

All data (DEMs, ERI profiles and DOI) are available in a Paraview project (Version 5.9.1) and can be downloaded via the following permanent link: https://cerema.box.com/v/SupDataVNCs2021. An enclosed "ReadMe.pdf" file explains how to display the project and provides also an algorithm and a Python code to compute the eroded and accumulated volumes of materials between the morphodynamic areas of two consecutive DEMs.

Declarations

Conflict of interest The authors declare no competing interests.

References

Agüera-Vega F, Carvajal-Ramírez F, Martínez-Carricondo P (2017) Assessment of photogrammetric mapping accuracy based on variation ground control points number using unmanned aerial vehicle. Measurement 98:221–227

Antoine R, Lopez T, Tanguy M, Lissak C, Gailler L, Labazuy P, Fauchard C (2020) Geoscientists in the sky: Unmanned aerial vehicles responding to geohazards. Surv Geophys 41(6):1285–1321. https://doi.org/10.1007/s10712-020-09611-7

Ayachit U (2015) The ParaView Guide: A Parallel Visualization Application. Kitware Inc, Clifton Park, NY, USA

Barnhart T, Crosby B (2013) Comparing two methods of surface change detection on an evolving thermokarst using high-temporal-frequency terrestrial laser scanning, Selawik River, Alaska. Remote Sensing 5:2813–2837. https://doi.org/10.3390/rs5062813

Boon DP, Chambers JE, Hobbs PR, Kirkham M, Merritt AJ, Dashwood C, Pennington C, Wilby PR (2015) A combined geomorphological and geophysical approach to characterising relict landslide hazard on the jurassic escarpments of Great Britain. Geomorphology 248:296–310

Boyd J, Chambers J, Wilkinson P, Peppa M, Watlet A, Kirkham M, Jones L, Swift R, Meldrum P, Uhlemann S, Binley A (2021) A linked geomorphological and geophysical modelling methodology applied to an active landslide. Landslides. https://doi.org/10.1007/s10346-021-01666-w

Brodu N, Lague D (2012) 3D terrestrial lidar data classification of complex natural scenes using a multi-scale dimensionality criterion: Applications in geomorphology. ISPRS J Photogram Remote Sens 68:121–134. http://www.sciencedirect.com/science/article/pii/S0924271612000330

Casella E, Rovere A, Pedroncini A, Mucerino L, Casella M, Cusati LA, Vacchi M, Ferrari M, Firpo M (2014) Study of wave runup using numerical models and low-altitude aerial photogrammetry: A tool for coastal management. Estuarine, Coastal and Shelf Science 149:160–167.

Chambers J, Wilkinson P, Kuras O, Ford J, Gunn D, Meldrum P, Pennington C, Weller A, Hobbs P, Ogilvy R (2011) Three-dimensional geophysical anatomy of an active landslide in Lias Group mudrocks, Cleveland Basin. UK. Geomorphology 125(4):472–484

Chesley J, Leier A, White S, Torres R (2017) Using unmanned aerial vehicles and structure-from-motion photogrammetry to characterize sedimentary outcrops: An example from the Morrison Formation, Utah, USA. Sediment Geol 354:1–8

Elhaï H (1963) La Normandie occidentale entre la Seine et le golfe normand-breton, étude morphologique, vol 40. Presses Universitaires de Rennes. https://www.persee.fr/doc/noroi_0029-182x_1963_num_40_1_1463_t1_0400_0000_4

Fuller IC, Large ARG, Heritage GL, Milan DJ, Charlton ME (2009) Derivation of Annual Reach-Scale Sediment Transfers in the River Coquet, Northumberland, UK, John Wiley & Sons, Ltd, pp 61–74. https://doi.org/10.1002/9781444304350.ch4, https://onlinelibrary.wiley.com/doi/pdf/10.1002/9781444304350.ch4

Fressard M, Maquaire O, Thiery Y, Davidson R, Lissak C (2016) Multi-method characterisation of an active landslide: Case study in the Pays d'Auge plateau (Normandy, France). Geomorphology 270:22–39

Giordan D, Adams MS, Aicardi I, Alicandro M, Allasia P, Baldo M, De Berardinis P, Dominici D, Godone D, Hobbs P, Lechner V, Niedzielski T, Piras M, Rotilio M, Salvini R, Segor V, Sotier B, Troilo F (2020) The use of unmanned aerial vehicles (uavs) for engineering geology applications. Bull Eng Geol Environ. https://doi.org/10.1007/s10064-020-01766-2

Göktürkler G, Balkaya Ç, Erhan Z (2008) Geophysical investigation of a landslide: The Altindağ landslide site, Izmir (western Turkey). J Appl Geophys 65(2):84–96

Goncalves J, Henriques R (2015) UAV photogrammetry for topographic monitoring of coastal areas. ISPRS J Photogram Remote Sens 104:101–111

Gonzalez-Ollauri A, Mickovski SB (2017) Shallow landslides as drivers for slope ecosystem evolution and biophysical diversity. Landslides 14(5):1699–1714

Grandjean G, Gourry J, Sanchez O, Bitri A, Garambois S (2011) Structural study of the Ballandaz landslide (French Alps) using geophysical imagery. J Appl Geophys 75(3):531–542

Gruszczynski W, Matwij W, Cwiakala P (2017) Comparison of low-altitude UAV photogrammetry with terrestrial laser scanning as data-source methods for terrain covered in low vegetation. ISPRS J Photogram Remote Sens 126:168–179

Günther T, Rücker C, Spitzer K (2006) Three-dimensional modelling and inversion of dc resistivity data incorporating topography-II Inversion. Geophys J Int 166(2):506–517

Hassen I, Fauchard C, Antoine R, Roulland T, Maquaire O, Costa S, Dugué O (2021) 3d geological modelling of a coastal area: case study of the Vaches Noires Cliffs, Normandy, France. Bull Eng Geol Environ 80(2):1375–1388. https://doi.org/10.1007/s10064-020-01955-z

Hirt C, Filmer MS, Featherstone WE (2010) Comparison and validation of the recent freely available ASTER-GDEM ver1, SRTM ver4.1 and GEODATA DEM-9S ver3 digital elevation models over Australia. Aus J Earth Sci 57(3):337–347. https://doi.org/10.1080/08120091003677553

Hobbs PRN, Jones LD, Kirkham MP, Holyoake SJ, Pennington CVL, Dashwood C, Banks VJ, Reeves HJ (2020) Establishment of a coastal landslide observatory at aldbrough, east riding of yorkshire, uk. Q J Eng Geol Hydrogeol 53(1):88–100

Huntley D, Bobrowsky P, Hendry M, Macciotta R, Elwood D, Sattler K, Best M, Chambers J, Meldrum P (2019) Application of multi-dimensional electrical resistivity tomography datasets to investigate a very slow-moving landslide near Ashcroft, British Columbia, Canada. Landslides 16(5):1033–1042. https://doi.org/10.1007/s10346-019-01147-1

Jaud M, Passot S, Le Bivic R, Delacourt C, Grandjean P, Le Dantec N (2016) Assessing the Accuracy of High Resolution Digital Surface Models Computed by PhotoScan ® and MicMac® in Sub-Optimal Survey Conditions. Remote Sens 8(6). https://doi.org/10.3390/rs8060465, https://www.mdpi.com/2072-4292/8/6/465

Jouniaux L, Maineult A, Naudet V, Pessel M, Sailhac P (2009) Review of self-potential methods in hydrogeophysics. Comptes Rendus Geosci 341(10):928–936. https://www.sciencedirect.com/science/article/pii/S1631071309001801

Lague D, Brodu N, Leroux J (2013) Accurate 3D comparison of complex topography with terrestrial laser scanner: Application to the Rangitikei canyon (N-Z). ISPRS J Photogram Remote Sens 82:10–26.http://www.sciencedirect.com/science/article/pii/S0924271613001184

Letortu P, Costa S, Maquaire O, Davidson R (2019) Marine and subaerial controls of coastal chalk cliff erosion in Normandy (France) based on a 7-year laser scanner monitoring. Geomorphology 335:76–91

Lebrun P, Courville P (2013) Le Jurassique des falaises des Vaches-Noires. Fossiles 4:16–27. https://hal-insu.archives-ouvertes.fr/insu-01133437

Lissak C, Maquaire O, Malet JP, Bitri A, Samyn K, Grandjean G, Bourdeau C, Reiffsteck P, Davidson R (2014) Airborne and ground-based data sources for characterizing the morpho-structure of a coastal landslide. Geomorphology 217:140–151

Loke M, Barker R (1996a) Rapid least-squares inversion of apparent resistivity pseudosections by a quasi-Newton method1. Geophys Prospect 44(1):131–152

Loke M, Barker R (1996b) Practical techniques for 3D resistivity surveys and data inversion. Geophys Prospect 44(3):499–523. https://onlinelibrary.wiley.com/doi/abs/10.1111/j.1365-2478.1996.tb00162.x

Maquaire O, Affchain P, Costa S, Lissak C, Fressard M, Letortu P, Davidson R (2013) Evolution á long terme des falaises des "Vaches Noires" et occurrence des glissements (Calvados, Basse-Normandie, France). In: Jounées Aléas Gravitaires, https://isterre.fr/IMG/pdf/maquaire.pdf

Marescot L, Monnet R, Chapellier D (2008) Resistivity and induced polarization surveys for slope instability studies in the Swiss Alps. Eng Geol 98(1):18–28

Medjkane M, Maquaire O, Costa S, Roulland T, Letortu P, Fauchard C, Antoine R, Davidson R (2018) High-resolution monitoring of complex coastal morphology changes: cross-efficiency of SfM and TLS-based survey (Vaches-Noires cliffs. Landslides, Normandy, France)

Merritt AJ, Chambers JE, Murphy W, Wilkinson PB, West LJ, Gunn DA, Meldrum PI, Kirkham M, Dixon N (2014) 3d ground model development for an active landslide in lias mudrocks using geophysical, remote sensing and geotechnical methods. Landslides 11(4):537–550. https://doi.org/10.1007/s10346-013-0409-1

Milan DJ, Heritage GL, Hetherington D (2007) Application of a 3D laser scanner in the assessment of erosion and deposition volumes and channel change in a proglacial river. Earth Surf Process Landforms 32(11):1657–1674

Oldenburg DW, Li Y (1999) Estimating depth of investigation in dc resistivity and ip surveys. Geophysics 64(2):403–416. https://doi.org/10.1190/1.1444545

Palis E, Lebourg T, Vidal M, Levy C, Tric E, Hernandez M (2017) Multiyear time-lapse ert to study short- and long-term landslide hydrological dynamics. Landslides 14(4):1333–1343. https://doi.org/10.1007/s10346-016-0791-6

Pazzi V, Morelli S, Fanti R (2019) A review of the advantages and limitations of geophysical investigations in landslide studies. Int J Geophys 2983087

Perrone A, Lapenna V, Piscitelli S (2014) Electrical resistivity tomography technique for landslide investigation: A review. Earth-Sci Rev 135:65–82

Peternel T, Kumelj S, Oštir K, Komac M (2017) Monitoring the Potoska planina landslide (NW Slovenia) using UAV photogrammetry and tachymetric measurements. Landslides 14(1):395–406

Petronio L, Boaga J, Cassiani G (2016) Characterization of the vajont landslide (North-Eastern Italy) by means of reflection and surface wave seismics. J Appl Geophys 128:58–67

Prodanovic D (2002) Terrain Analysis - Principles and Applications, John P. Wilson, John C. Gallant (Eds.), Wiley, New York, 2000, 479 pp (index included), hbk, isbn 0-471-32188-5. Urban Water 4(1):115, https://doi.org/10.1016/S1462-0758(01)00068-1, http://www.sciencedirect.com/science/article/pii/S1462075801000681

Quinejure E (1971) Formation superficielles et dynamique des bassins versants dans le Pays d'Auge. In: Colloque international de géomorphologie, p 27 p

Raeva PL, Filipova SL, Filipov DG (2016) Volume computation of a stockpile - a study case comparing gps and uav measurements in an open pit quarry. The International Archives of the Photogrammetry, Remote Sensing and Spatial Information Sciences XLI-B1:999–1004. https://doi.org/10.5194/isprs-archives-XLI-B1-999-2016. https://www.int-arch-photogramm-remote-sens-spatial-inf-sci.net/XLI-B1/999/2016/

Rosser N, Petley D, Lim M, Dunning S, Allison R (2005) Terrestrial laser scanning for monitoring the process of hard rock coastal cliff erosion. Q J Eng Geol Hydrogeol 38(4):363–375

Rossi G, Tanteri L, Tofani V, Vannocci P, Moretti S, Casagli N (2018) Multitemporal UAV surveys for landslide mapping and characterization. Landslides

Roulland T, Maquaire O, Costa S, Compain V, Davidson R, Medjkane M (2019) Analyse diachronique historique et récente á láide de documents multi-sources (Normandie, France). Géomorphologie: relief, processus, environnement 25(1):37–55

Roulland T, Maquaire O, Costa S, Medjkane M, Davidson R, Fauchard C, Raphaël A (2021) Seasonal activity quantification of coast badlands by tls monitoring over five years at the "vaches noires" cliffs (normandy, france). Geomorphology p. 108083. https://doi.org/10.1016/j.geomorph.2021.108083, https://www.sciencedirect.com/science/article/pii/S0169555X21004918

Rücker C, Günther T, Spitzer K (2006) Three-dimensional modelling and inversion of dc resistivity data incorporating topography - I. Modelling. Geophys J Int 166(2):495–505

Rücker C, Günther T, Wagner FM (2017) pygimli: An open-source library for modelling and inversion in geophysics. Computers & Geosciences 109:106–123

Stumpf A, Malet JP, Allemand P, Pierrot-Deseilligny M, Skupinski G (2015) Ground-based multi-view photogrammetry for the monitoring of landslide deformation and erosion. Geomorphology 231:130–145. https://www.sciencedirect.com/science/article/pii/S0169555X140060 0X

Telford WM, Geldart LP, Sheriff RE (1990) Applied Geophysics, 2nd edn. Cambridge University Press, Cambridge. https://doi.org/10.1017/cbo9781139167932, https://www.cambridge.org/core/books/applied-geophysics/FA576F8F33FCA4D56975BC58CE07851E

Turner IL, Harley MD, Drummond CD (2016) UAVs for coastal surveying. Coast Eng 114:19–24

Udphuay S, Güther T, Everett ME, Warden RR, Briaud JL (2011) Three-dimensional resistivity tomography in extreme coastal terrain amidst dense cultural signals: application to cliff stability assessment at the historic D-Day site. Geophys J Int 185(1):201–220

Viles H (2016) Technology and geomorphology: are improvements in data collection techniques transforming geomorphic science? Geomorphology 270:121–133

Whiteley JS, Chambers JE, Uhlemann S, Wilkinson PB, Kendall JM (2019) Geophysical monitoring of moisture-induced landslides: A review. Rev Geophys 57(1):106–145. https://agupubs.onlinelibrary.wiley.com/doi/abs/10.1029/2018RG000603

Zhou J, Revil A, Jardani A (2016) Stochastic structure-constrained image-guided inversion of geophysical data. GEOPHYSICS 81(2):E89–E101. https://doi.org/10.1190/geo2014-0569.1

Zhou J, Revil A, Karaoulis M, Hale D, Doetsch J, Cuttler S (2014) Image-guided inversion of electrical resistivity data. Geophys J Int 197(1):292–309. https://doi.org/10.1093/gji/ggu001

Cyrille Fauchard (✉) · Vincent Guilbert · Raphael Antoine · Cyril Ledun · Bruno Beaucamp
Research Team ENDSUM, Cerema, 10, chemin de la Poudrière, Le Grand Quevilly 76121, France
Email: cyrille.fauchard@cerema.fr

Olivier Maquaire · Stéphane Costa · Mohand Medjkane · Thomas Roulland
UMR 6554 LETG, Normandie University, Esplanade la Paix, Bât. A, Campus 1, Caen 14000, France

Olivier Maquaire
Email: olivier.maquaire@unicaen.fr

Stéphane Costa
Email: stephane.costa@unicaen.fr

Mohand Medjkane
Email: mohand.medjkane@unicaen.fr

Thomas Roulland
Email: thomas.roulland@unicaen.fr